

Is the average photon energy a unique characteristic of the spectral distribution of global irradiance?



G. Nofuentes^{a,b,*}, C.A. Gueymard^c, J. Aguilera^a, M.D. Pérez-Godoy^d, F. Charte^e

^aIDEA Research Group, University of Jaén, Campus de Las Lagunillas, 23071 Jaén, Spain

^bCentre for Advanced Studies in Energy and Environment, University of Jaén, Campus Las Lagunillas, 23071 Jaén, Spain

^cSolar Consulting Services, Colebrook, NH, USA

^dDepartment of Computer Science, University of Jaen, Campus Las Lagunillas, 23071 Jaén, Spain

^eDepartment of Computer Science and Artificial Intelligence, University of Granada, 18071 Granada, Spain

ARTICLE INFO

Article history:

Received 26 August 2016

Received in revised form 9 March 2017

Accepted 31 March 2017

Keywords:

Spectral irradiance

Solar spectral measurement

Average photon energy

ABSTRACT

The average photon energy (APE) has become a popular index to qualitatively assess whether shorter or longer wavelengths are enhanced in a specific spectral distribution of irradiance when compared to the AM1.5G standard spectrum. According to some previous assessments, this index might uniquely distinguish individual global tilted irradiance and global horizontal irradiance spectra. This paper basically applies the same methodology as that used in these studies, i.e., a statistical analysis based on spectral distributions grouped in 0.02-eV APE bins and their standard deviation across all 50-nm bands into which the wavelength range under scrutiny (350–1050 nm) is divided. Two years of spectral global tilted irradiance datasets collected at two Spanish locations, 333 km apart, are analyzed here. The same brand and model of spectroradiometer is used in each site with identical experimental protocols. It is found here that the coefficient of variation—a more meaningful statistical coefficient than the standard deviation to quantify dispersion around the mean—remains below 3.3% over the 450–900-nm waveband, whereas values up to 5–11% occur outside of it. It is shown that these higher values can be explained by the separate or combined impacts of experimental uncertainty and the direct effect of aerosols and water vapor. Based on radiative transfer principles related to these two atmospheric constituents, it is argued that APE cannot be a unique characteristic of the complete spectrum, thus confirming previous results that pertained to direct irradiance only. In practical terms, however, it is reasonable to ascertain that APE may be considered approximately unique relative to the spectrum distribution under the climate of the two sites under scrutiny over the limited 450–900-nm spectral range. This conclusion presumably holds for most of Spain, or even for locations with sunny inland climates similar to those of Jaén and Madrid.

© 2017 Elsevier Ltd. All rights reserved.

1. Introduction

The spectral distribution of incoming solar irradiance (in short, ‘spectral irradiance’) influences the performance of photovoltaic (PV) devices. Specifically, this influence occurs as a consequence of the differences between the actual solar spectrum under which the PV device operates and the specific standard solar spectrum used for rating purposes. Some PV technologies (e.g., those based on amorphous silicon or cadmium telluride) may be much more prone to such spectral effects than others (e.g., crystalline silicon). Consequently, the impact of the varying spectral irradiance has to be taken into account to achieve accurate predictions of the

expected energy to be delivered by such devices over long periods—during which the incident spectrum may change significantly. This spectral impact has been widely explored in literature and some valuable contributions date back to the 1980s and early 1990s (Pearsall et al., 1986; Wilson, 1986; Riordan and Hulstrom, 1990; Faine et al., 1991; Nann and Emery, 1992; Gonzalez and Carroll, 1994; Fabero et al., 1995). However, addressing this question remains an elusive goal, as detailed in the following paragraphs.

Spectrally-resolved irradiance observations are scarce, thus leading to studies using different experimental setups and/or time scales. Moreover, such studies tend to focus on a few well-equipped laboratories around the world, with results and conclusions not always easy to compare (Nann and Emery, 1992; Driesse et al., 2012; Sirisamphanwong and Ketjoy, 2012; Cornaro and Andreotti, 2012; Nofuentes et al., 2014; Alonso-Abella et al.,

* Corresponding author at: IDEA Research Group, University of Jaén, Campus de Las Lagunillas, 23071 Jaén, Spain.

E-mail address: gnofuen@ujaen.es (G. Nofuentes).

Nomenclature

Terminology

AERONET	Aerosol Robotic Network
CdTe	cadmium telluride
GHI	global horizontal irradiance
GTI	global tilted irradiance
IEC	International Electrotechnical Commission
NASA	National Aeronautics and Space Administration
PV	photovoltaic(s)

Symbols

a	lower wavelength limit of an interval of the spectrum (nm)
AM	air mass
APE	average photon energy (eV)
AOD	aerosol optical depth at any wavelength
AOD ₅₀₀	aerosol optical depth at 500 nm
b	upper wavelength limit of an interval of the spectrum (nm)
BF	blue fraction
CV	coefficient of variation (%)
$E(\lambda)$	spectral irradiance of the actual solar spectrum ($\text{W m}^{-2} \text{nm}^{-1}$)

MMF	spectral mismatch factor
PW	precipitable water (cm)
R_c	percentage contribution of a spectral band of a recorded spectral measurement to the broadband irradiance (%)
SD	standard deviation of R_c for every 50-nm band and the same APE interval (%)
SD _{max}	maximum value of standard deviation of R_c for every 50-nm band and the same APE interval (%)
SD _{mean}	Average value of standard deviation of R_c for every 50-nm band and the same APE interval (%)
SD _{min}	minimum value of standard deviation of R_c for every 50-nm band and the same APE interval (%)
SWF	spectrally weighted factor
U_{95}	expanded uncertainty related to spectral measurements (%)
UF	useful fraction
$\Phi(\lambda)$	spectral Photon Flux Density ($\text{m}^{-2} \cdot \text{nm}^{-1} \cdot \text{s}^{-1}$)
λ_{eff}	effective wavelength (nm)

2014; Ye et al., 2014; Dirnberger et al., 2015; Torres-Ramírez et al., 2015). Nevertheless, a recently publication (Gracia Amillo et al., 2015) is worthy of mention because of its global approach. Satellite-based solar radiation modeled data are resolved in spectral bands, which are then used to produce maps of the geographical variation of the solar spectrum.

In parallel, irradiance measurements recorded by means of a spectroradiometer are not common because of the cost and care needed to install and maintain such equipment, particularly on a temporally continuous basis. Such relatively rare measurements do not lend themselves well to engineering applications, since they are two-dimensional data whose characteristics depend on the instrument's spectral range of measurement, resolution, and accuracy. Consequently, identifying individual spectra by means of a single number or index can be highly useful to reduce the volume of such data and allow rapid comparisons between different periods at specific sites, or between different sites, etc. Indeed, many attempts in this direction have been carried out. For instance, Betts and co-workers (Betts et al., 2004) used the concept of 'useful fraction' (UF), defined as the ratio between the integrated spectral irradiance within the spectral response range of the considered PV device and the incident irradiance. Hofmann et al. (2013) proposed the spectrally weighted ratio (SWF), which takes into account both the whole solar spectrum and the external quantum efficiency of the solar cell. However, these parameters depend on the spectral response of the PV device. Similarly, the spectral mismatch factor (MMF), as stated in the IEC 60904-7 standard (IEC, 2008) is not well suited to accurately distinguish between each spectral distribution for the same reason. Alternatively, the blue fraction (BF) has been proposed to characterize the ratio between spectral irradiance integrated below 650 nm and the total irradiance (Sutterlueti et al., 2011). The possible bijective relationship between BF and spectrum shape is still under analysis, but already shows promising results (Louwen et al., 2016).

An older, and possibly better-known index, is the average photon energy (APE, in eV). A short review of the main literature devoted to the use of APE in flat-plate PV applications appears in Section 2. The present investigation is aimed at evaluating whether

the relationship between APE and spectral global tilted irradiance (GTI) may be assumed as reasonably bijective in practical terms, under a sunny inland climate, such as that of most of Spain. This experimental study uses two identical spectroradiometers at two separate locations representing two different sub-climates of Spain. The instruments are installed on equator-facing surfaces with the same tilt angle of 30° (slightly less than latitude, but reasonably close to the 37° standard value), with the aim to explore the impact on GTI's APE of a different geometry and experimental setup than those of previous studies. In this contribution, Minemoto et al.'s methodology (Minemoto et al., 2009)—which is to be detailed in what follows—is followed as closely as possible when analyzing the spectral data. The statistical analysis is conducted differently here, however, to gain better understanding on how well spectral irradiance instances with similar values of APE really conform to the same distribution.

2. Average photon energy (APE): Definition and state of the art

APE has been originally proposed by Jardine and co-workers (Jardine et al., 2002), who defined it as the mean energy value of all photons from a given solar spectrum distribution. In mathematical form:

$$\text{APE} = \frac{\int_a^b E(\lambda) d\lambda}{q \int_a^b \phi(\lambda) d\lambda} \quad (1)$$

where $E(\lambda)$ [$\text{W m}^{-2} \text{nm}^{-1}$] is the spectral irradiance, $\Phi(\lambda)$ [$\text{m}^{-2} \text{nm}^{-1} \text{s}^{-1}$] is the spectral photon flux density, q is the electronic charge, a [nm] and b [nm] are the lower and upper wavelength limits, respectively, of the considered waveband.

An equivalent definition is (Gueymard, 2009):

$$\text{APE} = hc(kq\lambda_{\text{eff}})^{-1} \quad (2)$$

with

$$\lambda_{\text{eff}} = \frac{\int_a^b \lambda E(\lambda) d\lambda}{\int_a^b E(\lambda) d\lambda} \quad (3)$$

where λ_{eff} is the “effective wavelength”, h is the Planck constant, c is the speed of light in vacuum, and k is a constant to reconcile units, equal here to 1×10^{-9} for λ_{eff} expressed in nm. The latter definition has the advantage of relating the possible variations in APE to even slight changes in the incident irradiance’s spectral balance. Intuitively, for instance, any atmospheric process yielding a red shift in the spectrum (conducive to larger λ_{eff}) is bound to decrease APE, whereas other conditions yielding a blue shift (shorter λ_{eff}) are bound to increase APE.

APE has been widely used in the scientific community thus far because it provides quantitative information on whether shorter or longer wavelengths are enhanced in a specific spectrum compared with the standard AM1.5G spectrum. APE was firstly hypothesized to be a *unique* characteristic of the solar spectrum by Minemoto et al. (2009). Their conclusion was based on a statistical analysis conducted using spectral GTI data collected over three years on an equator facing surface with a tilt angle of 15.3° in Kusatsu city, Japan (latitude 34°58’N, longitude 135°57’E). The methodology used by these authors was based on the criteria adopted by the International Electrotechnical Commission (IEC) to evaluate the spectral mismatch of a solar simulator (IEC 60904-9, 2007), itself defined by the deviation from the AM1.5G reference spectrum. Although these authors’ rationale is explained more in-depth hereafter, it can be roughly summarized as follows: If spectral distributions with nearly the same value of APE have a small standard deviation across all 50-nm bands into which the wavelength range under scrutiny is divided, such distributions may be assumed equal. Although a variety of results has been obtained based on this assumption (Takahashi et al., 2009; Minemoto et al., 2010; Nofuentes et al., 2013; Yoshida et al., 2013; Cornaro and Andreotti, 2012), it was often concluded that further research would be required elsewhere to verify the possible universality of this uniqueness feature.

In parallel, and basically following the same methodology as Minemoto et al., Norton et al. (2015) confirmed previous findings regarding the one-to-one relationship between APE and the shape of the spectrum. This conclusion resulted from their analysis of two spectrally-resolved global horizontal irradiance (GHI) experimental datasets obtained under the two contrasting climates of Ispra, Italy (latitude 45°49’N, longitude 8°36’E) and Golden, Colorado, USA (latitude 39°45’N, longitude 105°13’E). Measurements were taken during 16 months at the latter site and over two years at the former, using different instruments and dissimilar recording time intervals at each location. In any case, these authors also encouraged the collection and analysis of data elsewhere in order to validate their conclusions.

Recently, a study was carried out in Utrecht, The Netherlands (latitude 52°05’N, longitude 5°07’E, instruments installed on a 35°-tilted surface facing due south) by Louwen et al. (2016). They suggested using APE as a solid device-independent indicator of spectral variation on PV module performance, but did not make any conclusion about its possible uniqueness.

All the previous studies on APE were based on experimental data of either GHI or GTI at a few sites, making their results difficult to generalize and intercompare. A theoretical perspective might help resolve this issue. Such a study was conducted by Gueymard (Gueymard, 2009), using the SMARTS spectral irradiance model (Gueymard, 1995, 2001), which is a tool of choice to evaluate spectral effects on single- or multi-junction solar cells (Baig et al., 2016; Fernández et al., 2013; Myers and Gueymard, 2004; Virtuani et al., 2015). Following the author’s reasoning, and already alluded to above as a consequence of Eqs. (2) and (3), both air mass (AM) and aerosol optical depth (AOD) exert a similar influence on APE so that the spectrum shifts towards longer wavelengths when they increase, whereas precipitable water (PW) has a more limited but antagonistic effect. Then, at least theoretically, two different

sets of conditions (AM_1, AOD_1, PW_1) and (AM_2, AOD_2, PW_2) could lead to differing spectral distributions with the exact same value of APE. This leads to the conclusion that the APE of spectra measured over long periods of time at even a single site cannot be really unique in principle. However, the study focused on direct normal irradiance (DNI), which is known to be much more sensitive to both AM and AOD than GTI, or even more so, GHI. Thus, the finding just mentioned might not apply to the problem at hand. No similar theoretical study, focusing on GHI or GTI rather than DNI, has been found in the literature thus far. To remedy this situation, some theoretical considerations that are applicable to the present conditions are proposed in Section 3.

Interestingly, other doubts about the fundamental value of APE, but this time for GTI and on an experimental basis, were recently put forth by Dirnberger and co-workers (Dirnberger et al., 2015), who openly rejected APE as a unique characteristic of the spectrum distribution. Their analysis was based on a 3.5-year spectrally-resolved dataset from Freiburg im Breisgau, Germany (latitude 47°59’N, longitude 7°45’E, with instruments installed on a 35°-tilted surface facing due south). They concluded that APE is not a good index to quantify the spectral impact on single-junction devices.

The literature review just summarized clearly demonstrates that there are still various factors that need to be investigated before the hypothesis of APE’s bijective uniqueness can be accepted in the case of GTI or GHI, from either an experimental or theoretical perspective. What follows represents a step in the characterization of APE and its limitations, based exclusively on experimental data.

3. Materials and methods

3.1. Locations and experimental setup

The experimental campaign has been conducted at two Spanish sites: Jaén, (latitude 37°49’N, longitude 3°48’W, elev. 457 m, with a Mediterranean-Continental climate) and Madrid (latitude 40°24’N, longitude 3°44’W, elev. 665 m, with a Continental climate). Jaén is a non-industrialized, small-size city (116,000 inhabitants), periodically affected by Saharan dust episodes and high olive-tree pollen levels during May. In contrast, the city of Madrid has a much larger population (about 3.5 million) and suffers from pollution episodes and occasional Saharan dust intrusions. These locations (333 km apart) may be assumed representative of the general climate of the greater portion of Spain, with nuances. Key atmospheric information is obtained from ground-based observations from nearby sunphotometers belonging to the Aerosol Robotic Network (AERONET). The AERONET programme is a federation of ground-based sunphotometers established by the National Aeronautics and Space Administration (NASA), which started in the early 1990s (Holben et al., 1998). In Madrid, the AERONET site from the Spanish Meteorological Service (AEMET) is about 20 km away from the experimental site, and in a similar urban environment. For Jaén, the AERONET site of the University of Granada, 93 km to the south (latitude 37°10’N, longitude 3°36’W, elev. 680 m, with the same Mediterranean-Continental climate as Jaén) is close enough, so that values of atmospheric parameters of the latter are considered representative of the former, with however possible differences, as discussed below. Measurements of aerosol optical depth (AOD), precipitable water (PW) and other relevant atmospheric variables may be obtained from the AERONET database. Figs. 1 and 2 respectively show the seasonal variation of the daily mean and standard deviation of AOD₅₀₀—the aerosol optical depth at 500 nm in an atmospheric vertical column—and PW at Granada and Madrid.

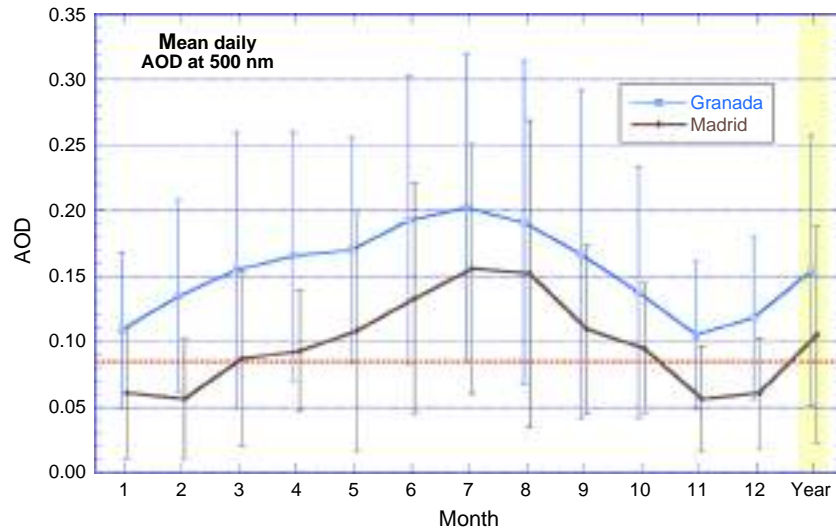


Fig. 1. Daily mean and standard deviation of aerosol optical depth at 500 nm (AOD_{500}) obtained from AERONET at Granada and Madrid on average for each month. The horizontal dashed line indicates the value (0.084) used to obtain the standard AM1.5G spectrum.

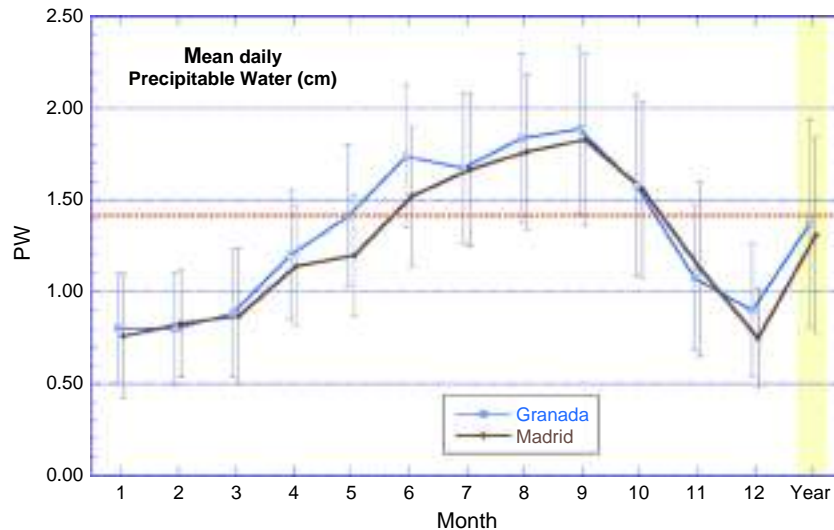


Fig. 2. Daily mean and standard deviation of precipitable water (PW) obtained from AERONET at Granada and Madrid on average for each month. The horizontal dashed line indicates the value (1.416 cm) used to obtain the standard AM1.5G spectrum.

Fig. 1 shows that AOD_{500} is significantly larger at Granada than Madrid. The magnitude of this difference was not anticipated, but can be explained by the more frequent and intense intrusions of Sahara dust over Granada, and by possibly more frequent pollution episodes due to the local topography that slows the dispersion of pollutants. It can thus be anticipated that AOD is somewhat lower at Jaén than Granada, with however a possible surge in May due to the intense pollen season.

The two figures display a characteristic seasonal variation, with higher values in summer, which is typical of temperate climates. Note that, in summer, AOD_{500} tends to be much larger than that of the standard AM1.5G spectrum at both sites, thus suggesting a smaller APE than the standard value. The reverse tends to be true in winter at Madrid, but not Granada. A similar wavy pattern emerges for PW at both sites, with however mean annual values very similar to that of the standard spectrum. This means that, on a seasonal-average basis, AOD and PW are the cause of antagonistic effects on APE, which can be also influenced by concomitant variations in the seasonal-average value of AM (lower in summer

and larger in winter). The standard deviation of daily values, also shown in Figs. 1 and 2, provides a measure of daily variability, which is significant, particularly for AOD—due in part to dust episodes.

The experimental data used in this work were collected from the outdoor research facilities located on the flat roof of one of the buildings of the High Technical School of the University Carlos III in Madrid and from those located on the flat roof of the Engineering and Technology building at the University of Jaén. These installations were described in detail in a previous study (Alonso-Abella et al., 2014).

At each site, the spectral irradiance was measured by means of a weatherproof EKO™ MS-700 grating spectroradiometer. Its specifications include a 10-nm spectral resolution and a temperature dependency of $\pm 1\%$ between -20 and $+50$ °C. The two instruments used in this study followed an identical experimental protocol, including a wavelength interval of 3.3 nm between 350 and 1050 nm, and acquisition every 5 min. The instruments were calibrated by the manufacturer before the experimental campaign,

and again after it, with no significant change in sensitivity. Additionally, the broadband GTI was measured with a Kipp & Zonen™ CMP 21 pyranometer. At each site, the spectroradiometer and pyranometer were mounted side by side on a south-facing plane with a tilt angle of 30° from horizontal. The experimental campaign lasted 24 months, from January 2011 to December 2013. An important data break, which lasted 15 days, occurred in August 2012 at the Madrid site. All spectra scanned while the broadband GTI was below 300 W m⁻² were excluded, thus avoiding the noise introduced by low irradiances. This should be of no concern in the subsequent analysis, since the PV output under such low irradiance levels is almost irrelevant at sunny sites such as those under scrutiny in this work (Wilk, 1997; Hegedus and Luque, 2003; Nofuentes et al., 2009, 2013, 2014; Torres-Ramírez et al., 2014).

3.2. Methodology

It is known that APE is an index that provides a qualitative comparison of spectral conditions so that the higher the APE, the lower λ_{eff} and the blue content of light. This index is calculated by dividing the incident irradiance by the total photon flux density, per Eq. (1) above, or alternatively through Eqs. (2) and (3). In those equations, the values for a and b are imposed by the model of spectroradiometer used here, i.e., 350 and 1050 nm. It is important to specify these values since, according to Eqs. (1)–(3), APE directly depends on them for any given spectrum. For the conditions of the AM1.5G reference spectrum, for instance, APE equals 1.88 eV for the 350–1050 nm range (Minemoto et al., 2007) vs. 1.59 eV for the extended 350–1700 nm range (Ishii et al., 2013).

As commented in Section 1, the methodology initially proposed by Minemoto et al. (2009) is followed as closely as possible in this investigation, in order to assess the possible bijective relationship between a given APE value and the GTI spectral shape. Overall, the main steps of the APE analysis procedure used here are summarized as follows:

- (1) The broadband irradiance is obtained between 350 and 1050 nm for each spectral measurement, using the trapezoidal rule.
- (2) The APE is calculated for each spectral measurement by means of Eq. (1).
- (3) The wavelength range is divided into fourteen 50-nm bands for each spectral scan. Then, the percentage contribution, R_c , of each spectral band to the broadband irradiance calculated in step 1 is obtained.
- (4) All the spectral measurements are binned into 0.02-eV width APE intervals according to the latter's value. Eight intervals ranging from 1.78–1.80 eV to 1.92–1.94 eV are considered. Each of these intervals contains spectral measurements lying within ± 0.01 eV of its central value.
- (5) For every APE interval, spectral measurements with values of R_c below the 10th percentile or above the 90th percentile are discarded within each 50-nm band. Thus, the results of the analysis are less subject to the influence of outliers.
- (6) Mean values of R_c , $\langle R_c \rangle$, in each 50-nm band are calculated for every APE interval. The standard deviation, SD, along with the coefficient of variation, CV (stated as the percentage ratio of SD to $\langle R_c \rangle$), are also calculated for each of these bands to determine the scatter in the values of R_c around its mean value for every APE interval.

4. Results and discussion

As commented in step 4 of the methodology described just above, eight APE intervals are considered, ranging from 1.79 ± 0.01 eV to 1.93 ± 0.01 eV. The reason behind this limited

range of APE values is that spectral measurements falling outside of these intervals account for less than 0.5% of the total spectral instances collected over the course of the experimental campaign. After all the filtering just described, 34,503 and 40,554 spectral samples remained in the datasets from Jaén and Madrid, respectively.

It is worth investigating whether the reference spectrum is really representative of local conditions. In this respect, it should be remembered that the AM1.5G standard spectrum refers to a sun-facing plane surface tilted at 37° to the horizontal, close to the geometry of the spectroradiometers installed in Jaén and Madrid. Therefore, it is worthwhile to check whether the local spectral distribution, for APE and AM close to 1.88 eV and 1.5, respectively, resembles that of the standard. Fig. 3 depicts the values of $\langle R_c \rangle$ for the fourteen 50-nm bands considered in this work, calculated for spectral measurements with APE and AM ranging from 1.87 to 1.89 eV and 1.45 to 1.55, respectively. This is done for data collected at both Jaén and Madrid. The percentage contributions of every band to broadband irradiance integrated between 350 and 1050 nm are also shown for the reference spectrum. Apparently, it seems that the “local all-weather” AM1.5G distributions for Madrid and Jaén closely resemble that of the standard (which specifically characterizes clear-sky conditions only), on average. This statement must be nuanced due to some discernible variability along the spectrum, however. Despite not being easily noticed in Fig. 3, the (normally small) values of SD are not negligible when compared to those of $\langle R_c \rangle$ in the 50-nm bands that lie within 350–450 nm and 900–1050 nm for both sites. This fact obviously denotes larger scatter of percentage contributions outside the central band (450–900 nm) for this set of spectral measurements. This issue is dealt with quantitatively hereafter.

The mean R_c values for every 50-nm band according to each APE interval for the spectral measurements recorded in Jaén and Madrid are depicted in Figs. 4 and 5, respectively. The values of AM corresponding to such data are in the range 1.03–6.51 at Jaén and 1.03–6.53 at Madrid. Their overall mean values are 1.77 and 1.78 at Jaén and Madrid, respectively, thus significantly higher than the standard 1.5 value. In parallel, the mean broadband GTI values are 729 and 677 W m⁻², respectively, thus much lower than the 1000 W m⁻² standard value (even though all GTI values below the 300 W m⁻² threshold were discarded).

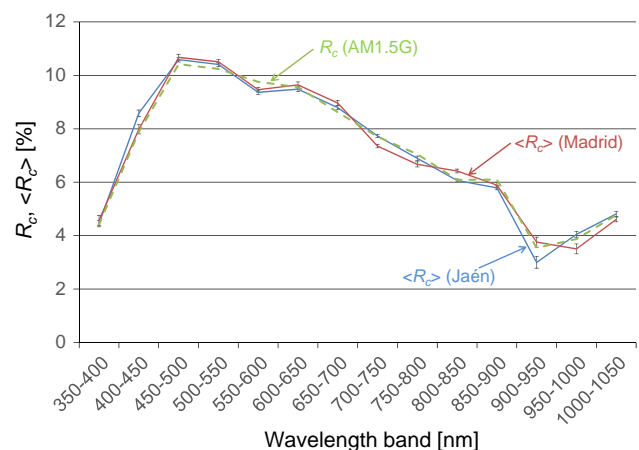


Fig. 3. Mean values of R_c for every 50-nm band in spectral measurements with APE and AM confined within 1.88 ± 0.01 eV and 1.50 ± 0.05 , respectively, recorded in Jaén (blue line) and Madrid (red line). Error bars indicate the values of SD related to each of these bands. Values of R_c calculated in each of these bands for the AM1.5G spectrum are also shown (green dashed line). (For interpretation of the references to colour in this figure legend, the reader is referred to the web version of this article.)

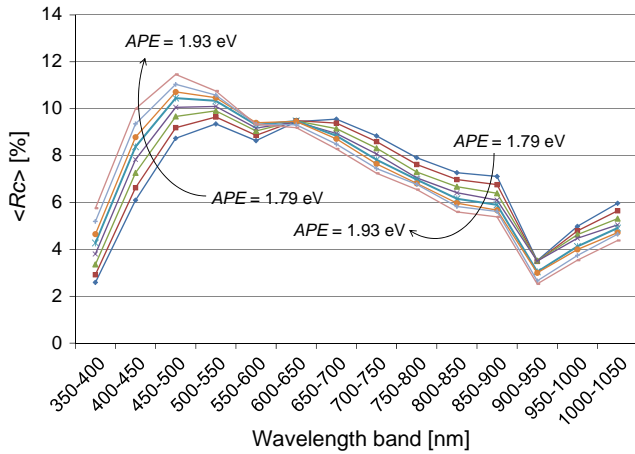


Fig. 4. Mean values of R_c in every 50-nm band for spectral measurements grouped in 0.02-eV width of APE intervals over the range 1.79–1.93 eV (central values) for spectral data recorded in Jaén.

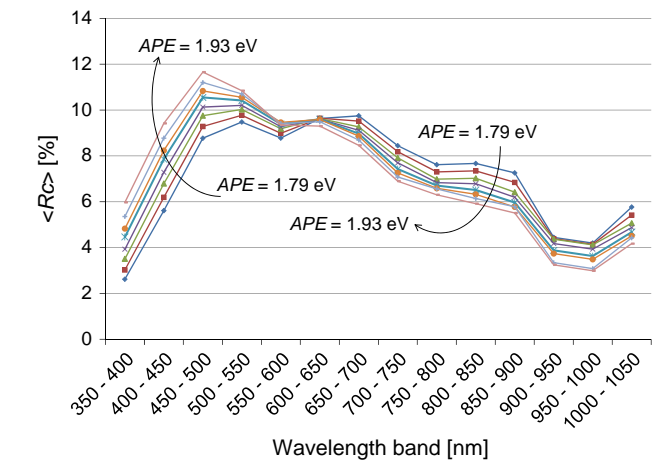
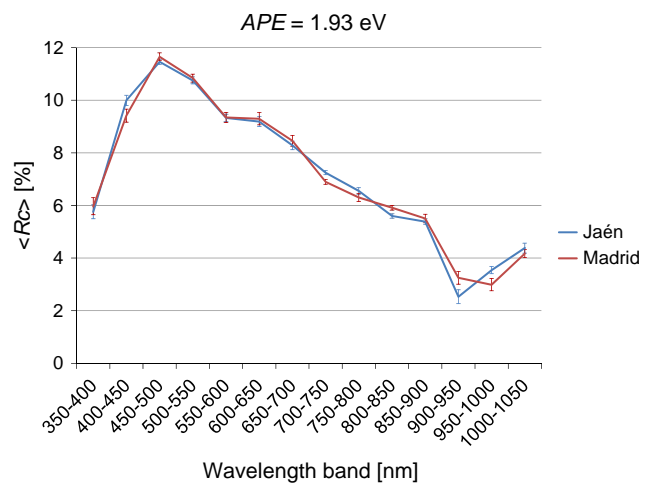
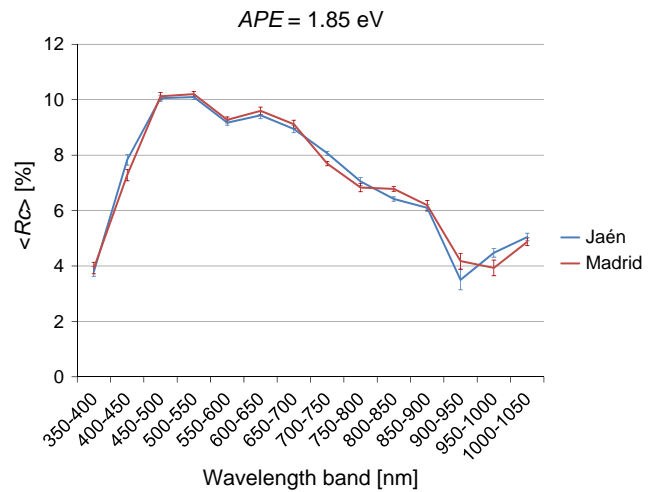
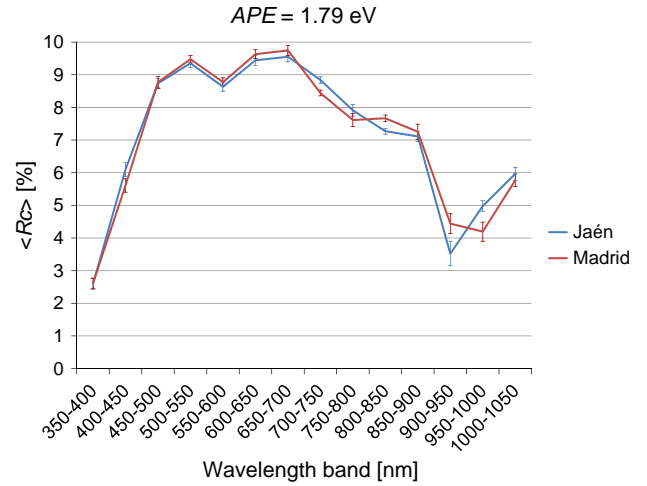


Fig. 5. Mean values of R_c in every 50-nm band for spectral measurements grouped in 0.02-eV width of APE intervals over the range 1.79–1.93 eV (central values) for spectral data recorded in Madrid.

The mean R_c values for every 50-nm band according to each APE interval for the spectral measurements recorded in Jaén and Madrid are depicted in Figs. 4 and 5, respectively. As could be expected, the higher the APE, the smaller λ_{eff} , and the higher the percentage contribution to the integrated irradiance in 50-nm bands with shorter wavelengths. Conversely, lower values of APE lead to higher values of such percentage contributions in 50-nm bands with longer wavelengths. A small and nearly constant value of (R_c) appears in the 600–650-nm spectral band, which corresponds to a stable and “ideal” spectral balance for the 350–1050-nm waveband at the present experimental sites. These results are quite well aligned with those obtained by Minemoto et al. for Kusatsu city (Japan) and Norton et al. for Ispra (Italy) and Golden, Colorado (USA).

Fig. 6 shows the good match that is achieved between values of (R_c) obtained across all the 50-nm bands for three specific APE intervals at Jaén and Madrid. Despite not being depicted, this agreement between the mean values of the above percentage contributions calculated at both sites within the 350–1050 nm waveband also holds for the five remaining data sets grouped according to their APE value. However, two important comments must be made at this point. First, the largest discrepancies between values of (R_c) for Madrid and Jaén occur within 900–1000 nm. Such discrepancies also occur within this band at the two sites analyzed

Fig. 6. Mean R_c values in every 50-nm band for spectral measurements with APE confined within 1.79 ± 0.01 eV (top), 1.85 ± 0.01 eV (middle) and 1.93 ± 0.01 eV (bottom), recorded in Jaén (blue line) and Madrid (red line). Error bars indicate the values of SD related to each 50-nm band. (For interpretation of the references to colour in this figure legend, the reader is referred to the web version of this article.)

by Norton et al. Second, as previously mentioned, values of SD outside the 450–900-nm waveband are not negligible when compared to those of (R_c), as the analysis below underlines. This fact is especially noticeable within the 900–1000 nm band as well, which corroborates the results of Norton et al. at Ispra and Golden.

Tables 1 and 2 gather the distribution of the spectral measurements grouped by their corresponding APE interval for Jaén and Madrid, respectively. The corresponding effective wavelengths, as well as the maximum, minimum, and mean values of SD related to R_c across all 50-nm bands for each APE group are also shown in both Tables. It is worth mentioning that, for both Jaén and Madrid, 71% of the spectral measurements are concentrated within only two intervals: 1.87 ± 0.01 eV and 1.89 ± 0.01 eV. Indeed, the number of measurements binned in all APE intervals dramatically falls off when the central values of the latter move away from 1.88 eV. As could be expected from statistical principles, higher values of SD occur in APE groups that contain fewer samples. Thus, it is found that data sets binned into intervals corresponding to each end of the APE range under scrutiny show the largest dispersion. In any case, these values of SD do not exceed 0.37% and 0.32% in Jaén and Madrid, respectively.

Values of the standard deviation of R_c across all the 50-nm bands gathered in Tables 1 and 2 are quite similar to those obtained by Minemoto et al. for Kustasu city, but smaller than those calculated by Norton et al. for Ispra and Golden. The maximum SD values for these three cities were 0.39%, 1.29% and 1.35%, respectively. However, a suitable quantitative assessment of how well each APE data set conforms to the mean values of the percentage contributions across all the 50-nm bands requires a more meaningful metric than SD for the purpose of this work. It is argued here that CV is more discriminant than SD in the present context. In particular, Figs. 7 and 8 depict the values of CV for every 50-nm band according to each APE interval for the Jaén and Madrid data, respectively. The two figures exhibit a similar shape so that they can be jointly interpreted. Interestingly, values of CV within the 450–900-nm waveband are found to remain below a low boundary of $\approx 3.3\%$. In principle, this suggests that APE can be assumed uniquely linked—at least in practical terms—to any specific spectral distribution of GTI. In contrast, significantly larger variability exists within 350–450 nm, where CV values above 5% appear. Much steeper spikes are also noticed in the 900–1050-nm waveband, where CV reaches up to 6–11% depending on wavelength interval and location. The potential causes for these spikes need to be better understood. The discussion below provides important elements of explanation, based on a critical review of the experimental and atmospheric conditions at play.

According to the certificate of calibration issued by the manufacturer, the expanded uncertainties (U_{95}) for the spectral measurements obtained with Jaen's instrument are as follows: $\pm 10.90\%$, $\pm 4.20\%$, and $\pm 4.10\%$ for the 350–450 nm, 450–900 nm and 900–1050 nm wavebands, respectively. Similar numbers apply to the Madrid instrument: $\pm 10.77\%$, $\pm 4.10\%$, and $\pm 4.04\%$, respectively. The higher values of U_{95} below 450 nm (due mostly to stray light, which accounts for half of the uncertainty in that band) help explain the scatter noticed for R_c at these shorter wavelengths and the concomitant higher values of CV. Counter-intuitively, the lowest U_{95} values are reported above 900 nm (where CV is the largest), which requires explanation. It should be kept in mind that the two

spectroradiometers used here underwent their calibration procedure in a laboratory at constant ambient temperature (25 °C), thus avoiding most complications that result from field operation. Indeed, large temperature excursions typically occur during sunny days, thus impacting the reading accuracy in the NIR part of the spectrum much more than in shorter wavebands (Myers, 1989; Schubert et al., 2015). Moreover, the spectral irradiance is naturally weak within the water vapor absorption band (around 940 nm), and hence measurements in that band are more vulnerable to noise.

From the measurand standpoint now, PW at any site tends to be variable on a daily basis, and even on a hourly basis, due to more or less rapid fluctuations in weather conditions, as shown in Fig. 9 for Granada and Madrid; see also (Gueymard, 2014) for more context. This natural variability in PW leads to highly variable water vapor absorption around 940 nm, which also happens to be the strongest absorption band over 350–1050 nm. The atmospheric transmittance in that absorption band is proportional to $(AM \cdot PW)^c$, where the value of exponent c is ≈ 0.58 (Mavromatakis et al., 2007 and references therein). In Granada, the 5th and 95th percentiles of the AERONET PW data were 0.507 and 2.353 cm (a 4.6X increase), respectively, during 2004–2015. A similar range (0.506 and 2.189 cm, respectively) is found at Madrid during the much shorter period 2012–2015. Consequently, with 90% certainty, the possible range of temporal change in irradiance that can be expected at the experimental sites over the 940-nm band is $\approx 4.6^{0.58}$ or about 2.4X, when considering a constant air mass of 1.5 for the sake of this simple example (in reality, AM is variable, thus compounding the issue). This result is confirmed in Fig. 10, which compares the predicted GTI for the two extreme PW values just mentioned for Granada and for the AM1.5G standard conditions ($PW = 1.416$ cm), based on SMARTS v2.9.5 calculations. These include a call to its post-processor to simulate the output of the present type of spectroradiometer, i.e., using a 10-nm resolution (full width at half maximum with Gaussian shape); see Gueymard (2001) for details on this procedure.

The large impact of water vapor absorption alone can explain the noticeable variability of CV in the 900–950-nm waveband noted above. The difficulty of obtaining “good” results beyond 900 nm was also noted by Norton et al. when assessing the one-to-one relationship between APE and spectral shape at Ispra and Golden.

At the other end of the observed spectrum, i.e. in the 350–450 nm waveband, there is no measurable absorption due to water vapor or other gases. Hence, the only variable atmospheric factor of interest, at least under clear skies, is AOD. Although its impact on GTI can be expected to be smaller than that on DNI, which was discussed by Gueymard (2009), it still deserves further scrutiny. Similarly to Fig. 10, Fig. 11 represents the SMARTS-simulated spectral tilted irradiance between 350 and 500 nm that pertain to different cases: The AM1.5G standard spectrum, and the near-extreme (5th and 95th percentiles) AOD₅₀₀ conditions at Granada and Madrid, all obtained for a fixed air mass of 1.5 and smoothed to the instru-

Table 1
Maximum, minimum, and mean values of SD of R_c for every 50-nm band according to their APE interval for Jaén.

Central value of APE interval (eV)	λ_{eff} corresponding to the central value of APE interval (nm)	SD _{max} (%)	SD _{min} (%)	SD _{mean} (%)	# Samples	Waveband where SD _{max} occurs	Waveband where SD _{min} occurs
1.79	693	0.37	0.09	0.17	426	900–950	800–850
1.81	685	0.37	0.09	0.16	968	900–950	800–850
1.83	678	0.37	0.08	0.16	2273	900–950	800–850
1.85	670	0.36	0.07	0.14	5772	900–950	700–750
1.87	663	0.31	0.07	0.14	8605	900–950	800–850
1.89	656	0.23	0.05	0.10	15,908	900–950	700–750
1.91	649	0.24	0.06	0.14	485	350–400	700–750
1.93	642	0.26	0.08	0.15	66	350–400	700–750

Table 2
Maximum, minimum, and mean values of SD of Rc for every 50-nm band according to their APE interval for Madrid.

Central value of APE interval (eV)	λ_{eff} corresponding to the central value of APE interval (nm)	SD _{max} (%)	SD _{min} (%)	SD _{mean} (%)	# Samples	Waveband where SD _{max} occurs	Waveband where SD _{min} occurs
1.79	693	0.30	0.09	0.18	756	900–950	700–750
1.81	685	0.29	0.09	0.17	1681	900–950	700–750
1.83	678	0.26	0.08	0.16	4420	900–950	700–750
1.85	670	0.29	0.08	0.16	6550	900–950	700–750
1.87	663	0.27	0.09	0.16	11,246	900–950	700–750
1.89	656	0.22	0.06	0.12	14,448	900–950	700–750
1.91	649	0.27	0.08	0.17	1198	350–400	700–750
1.93	642	0.32	0.09	0.19	255	350–400	700–750

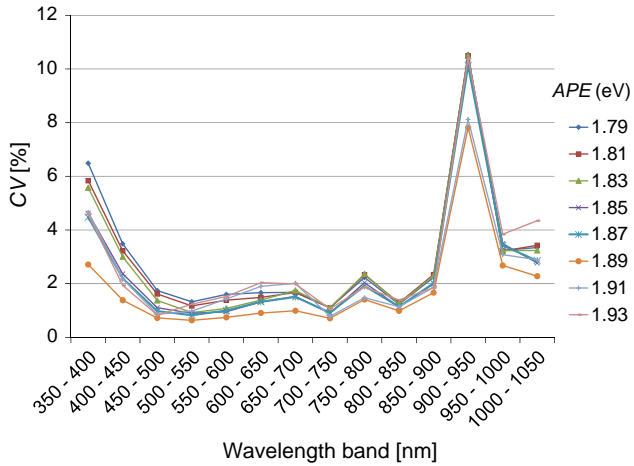


Fig. 7. Coefficient of variation of Rc of every 50-nm band for spectral measurements grouped into 0.02-eV-width APE intervals over the range 1.79–1.93 eV (central values) for spectral data recorded in Jaén.

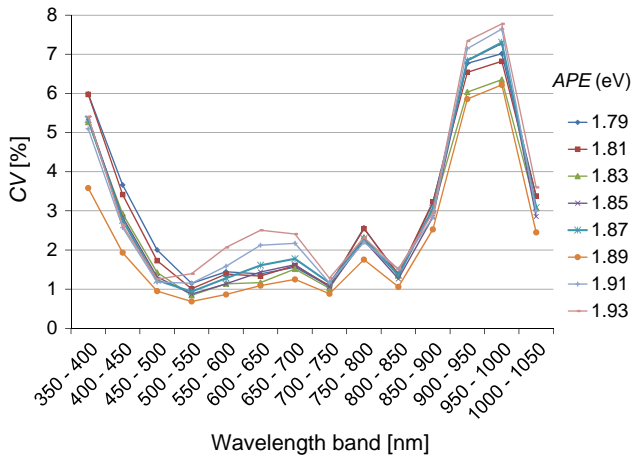


Fig. 8. Coefficient of variation of Rc of every 50-nm band for spectral measurements grouped into 0.02-eV width APE intervals over the range 1.79–1.93 eV (central values) for spectral data recorded in Madrid.

ment’s 10-nm resolution. The absolute difference between the AM1.5G and the near-extreme conditions is here much less than around 940 nm. Interestingly, though, this absolute difference does not change much when wavelength decreases from 500 to 350 nm, while GTI strongly decreases, conducive to a progressively larger relative difference. Note also the interesting stair-like shape of the spectral GTI, with sharp declines around the 450 and 400 nm steps compared to the 450–500 nm waveband. The progressive increase of the relative impact of AOD on GTI when wavelength

decreases below 500 nm is consistent with the concomitant increase in CV shown in Figs. 7 and 8. Like with Fig. 10, these effects would be compounded by letting AM vary to represent realistic conditions.

From a different perspective, radiative transfer theory shows that the aerosol-induced effects on GTI at any wavelength λ are, like with DNI, a strong function of the product $AM \bullet AOD$. The value of AOD at any wavelength λ is itself a strong function of AOD_{500} through Ångström’s law, even though the exact average size of the aerosol mixture (which may change over time and space) introduces some variance in the ratio between the two quantities. This theoretical development indicates that, below 500 nm, variable $V_1 = AM \bullet AOD_{500}$ may account for nearly all the natural GTI variability in that part of the spectrum. This complements the previous findings about the spectrum beyond 900 nm, which is essentially affected by variable $V_2 = AM \bullet PW$.

Variables V_1 and V_2 affect the magnitude of APE in antagonistic ways, but also *qualitatively* affect the shape of the GTI spectrum in very different ways. A combination $(V_1, V_2)_1$ of the two driving variables might lead to a blue-shifted spectrum, whereas the combination $(V_1, V_2)_2$ might result in a red-shifted spectrum, even though they have the exact same APE in common. For this simple reason, it is established that, from a pure theoretical standpoint, APE *cannot* be a unique feature of the GTI spectrum, thus generalizing the findings of Gueymard (2009). From a more pragmatic standpoint, however, the low CV noticed above between 450 and 900 nm leads to the reasonable conclusion that, *in practice and for the specific sites considered here*, APE can be considered an *approximately* unique feature of this central part of the spectrum. This finding presumably applies to most of Spain, or even to locations experiencing sunny inland climates similar to Jaén’s and Madrid’s.

The leading role of V_1 and V_2 in the differential shaping of the spectrum for a unique value of APE means that the pragmatic conclusion reached above might have climatic overtones. For future reference, the cloud of paired observations of V_1 and V_2 at Granada is shown in Fig. 12. Note that, because of the AERONET observational procedure, AM is always limited to a maximum value of 5, whereas the present experimental data sets contain a significant number of instances with AM between 5 and ≈ 6.5 . The actual locus would thus be larger under the present experimental conditions at Jaén and Madrid.

The present results are consistent with those of Dirnberger et al. (2015), who studied the behavior of MMF vs. APE for most single junction PV technologies. They concluded that MMF is more sensitive to the spectrum shape than APE thus resulting in different values of the former parameter for the same value of the latter. In particular, they came to the interesting conclusion that spectral measurements yielding values of APE similar to that corresponding to the AM1.5G standard (1.88 eV) do not necessarily produce values of MMF very close to 1—as they should if the relationship APE-spectrum shape were bijective. Although the work of Dirnberger et al. does not explore this issue waveband by waveband, it basically supports the present finding that APE cannot be

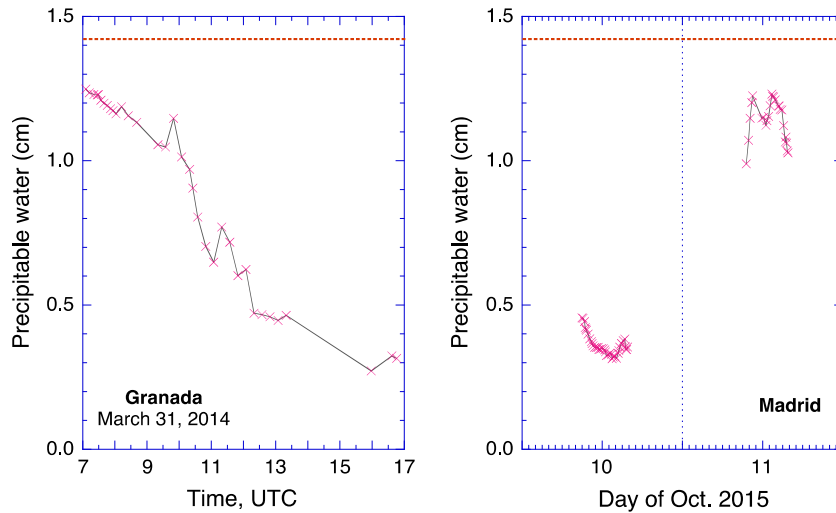


Fig. 9. Left: Variation of PW measured with an AERONET sunphotometer during a single day at Granada. Right: Variation of PW measured with an AERONET sunphotometer during two successive days at Madrid. The horizontal dashed line indicates the specific value of PW (1.416 cm) corresponding to the AM1.5 standard spectrum.

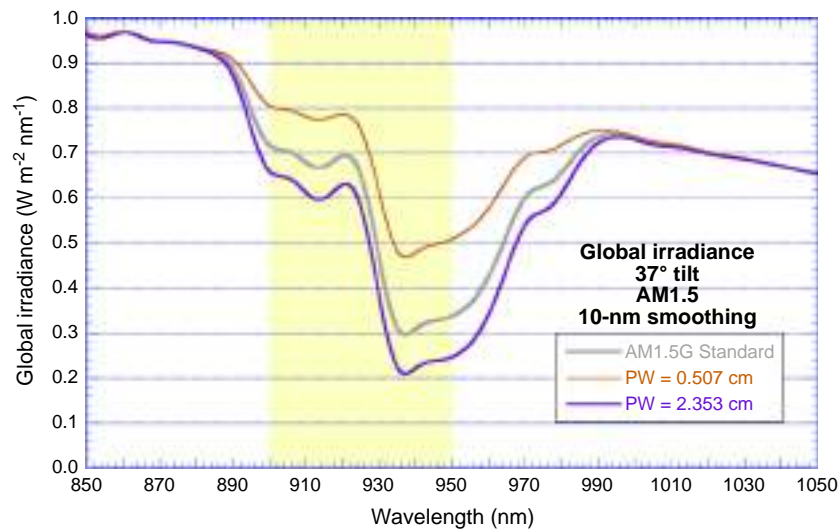


Fig. 10. Global tilted irradiance simulated with SMARTS for a 37°-tilted surface facing the sun under standard conditions, and under “near-extreme” PW conditions at Granada. The irradiance is smoothed to simulate the output of the present spectroradiometer make and model. The yellow area indicates the 900–950-nm waveband, which is most impacted by water vapor absorption. (For interpretation of the references to colour in this figure legend, the reader is referred to the web version of this article.)

considered unique to each spectral distribution over the full 350–1050 nm range.

To summarize, the above discussion justifies the rejection, even in practical terms, of the APE uniqueness to the spectral GTI distribution outside of the 450–900 nm central band at Jaén and Madrid. This rejection may hold for other sites with similar sunny inland climates such as those of the two sites analyzed here. Further research would be needed, however, to elucidate how general this conclusion can be asserted, depending on the climatic variability of the critical variables V_1 and V_2 at other sites.

5. Conclusions

The aim of the present experimental study is to assess whether APE can be used as an index that uniquely describes the spectral GTI at two Spanish inland sunny sites (Jaén and Madrid). The methodology adopted here is based on the criteria used by the International Electrotechnical Commission to evaluate the spectral

match of a solar simulator to the AM1.5G spectrum. This is similar to what was used before in previous studies conducted at a few other sites over three continents. However, the statistical analysis is expanded here by analyzing the coefficient of variation—in addition to the mean and standard distribution—of the percentage contributions of 50-nm bands to the integrated irradiance of the spectral distributions grouped in a specific APE interval.

Spectral irradiance distributions at the two Spanish sites under scrutiny were measured between 350 and 1050 nm with the same type of spectroradiometer during a period of 24 months. Spectral distributions of measurements corresponding to values of APE close to 1.88 eV for AM maintained at 1.50 ± 0.05 closely resemble that of the standard AM1.5G spectrum within 450–900 nm, whereas some scatter is noticed outside of this band. Likewise, spectral distributions corresponding to measurements binned in the same APE interval strongly agree within 450–900 nm since the coefficient of variation remains below 3.3% in that waveband. However, this coefficient reaches significantly larger values, about 6% and 11%, within 350–450 nm and 900–1050 nm, respectively.

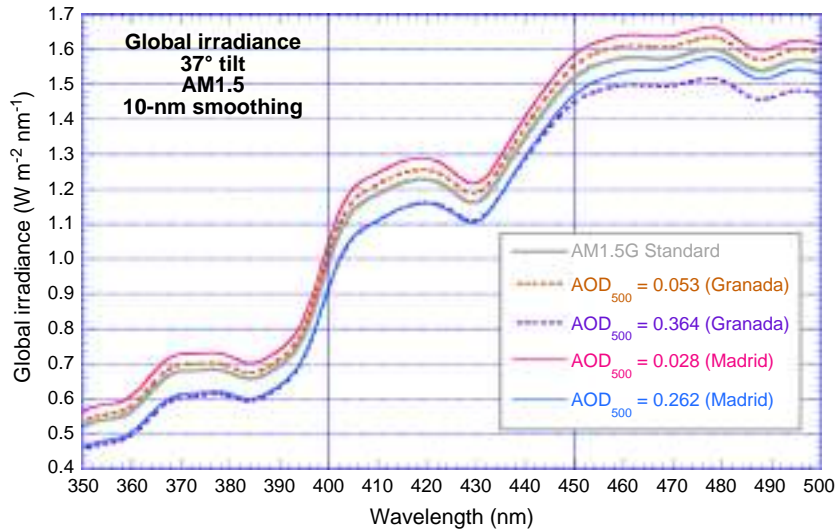


Fig. 11. Global tilted irradiance simulated with SMARTS for a 37°-tilted surface facing the sun under standard conditions, and under “near-extreme” AOD conditions at Granada and Madrid. The irradiance is smoothed to simulate the output of the present spectroradiometer make and model. The vertical lines indicate the 50-nm waveband limits at 400 and 450 nm.

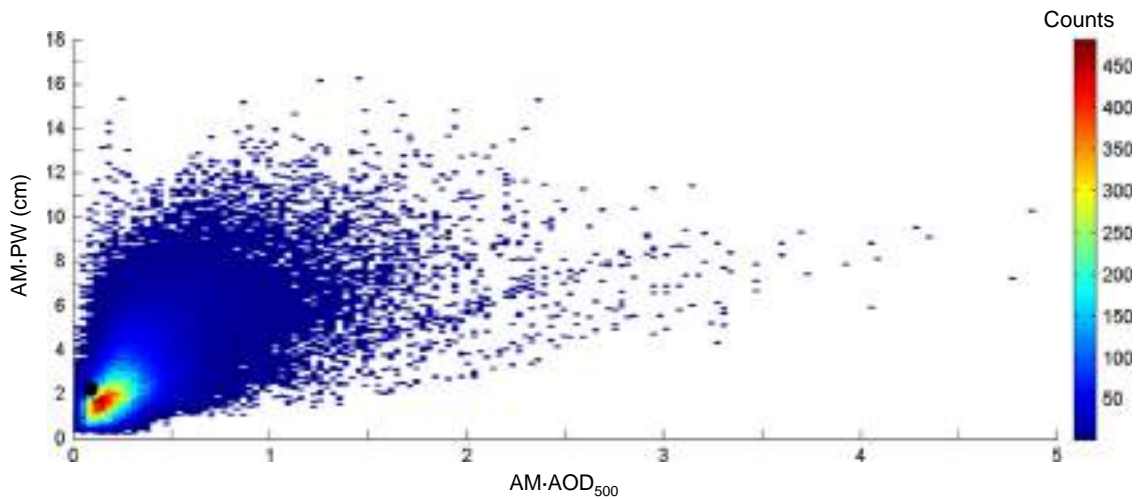


Fig. 12. AERONET observations of $V_1 = AM * AOD_{500}$ and $V_2 = AM * PW$ at Granada during 2004–2015 for $AM \leq 5$. The black dot indicates the AM1.5G standard conditions.

The largest experimental uncertainty, according to the instrument’s calibration certificate, occurs in the former band, but measurements over the near infrared can be affected by steep temperature excursions during the day. This can affect the accuracy of the results, particularly in the 940-nm water vapor absorption band, where the low signal tends to increase the noise level. The significant temporal variability in PW is another source of uncertainty in the near-infrared band. The present findings suggest that this temporal variability and the intense water vapor absorption around 940 nm are actually the main source of concern for that band. Similarly, it is demonstrated that natural daily variations in AOD tend to affect the GTI spectrum mostly below 450 nm, and increase variability there. All this strongly suggests that the two main atmospheric factors (aerosols and water vapor), exclusive of clouds, that are the most variable spatially are also those that have the most impact on the spectral distribution below 450 nm and above 900 nm, and thus the most impact on the temporal variability of APE within these bands. Based on radiative transfer principles, it is shown that the two critical variables that affect both the magnitude of APE and the qualitative shape of the two ends of the experimental spectrum are $V_1 = AM * AOD_{500}$ and

$V_2 = AM * PW$, and that the uniqueness of APE cannot be accepted from a pure theoretical standpoint, thus confirming previous findings that pertained to the direct spectrum only. The temporal variability of the antagonistic effects caused by aerosols and water vapor, the anticipated additional (but presumably small) impact of clouds, and the concomitant changes in the effective wavelength of the spectrum (leading to changes in APE), would have to be addressed in a more general study encompassing many different aerosol, water vapor, and cloud regimes.

The noted scatter in the present results outside of the 450–900-nm band seem to confirm some previous findings, and leads to the conclusion that a bijective relation between APE and global tilted irradiance spectra cannot be reasonably assumed at the sites studied over the complete 350–1050-nm waveband. Since the largest discrepancies take place beyond 900 nm, where PV technologies such as amorphous silicon or CdTe do not absorb sunlight, it is virtually impossible to correctly evaluate their temporal spectral effects relative to standard conditions with APE alone, for instance.

In summary, the present results indicate that APE may be reasonably uniquely linked to the spectral distribution of GTI between 450 and 900 nm *only approximately* and from a pragmatic perspec-

tive, i.e., for the general conditions of Jaén and Madrid and presumably most of Spain or even for locations with similar sunny inland climates. Uniqueness is, however, remarkably almost “perfect” over the short interval 600–650 nm, which corresponds to the effective wavelength of the 350–1050-nm waveband under scrutiny here. Based on the present findings, only the restrictive 450–900-nm APE can be recommended in all future studies devoted to the application of APE to spectral effects in tilted flat-plate PV.

Acknowledgements

The authors sincerely thank the financial support provided by the Spanish Science and Innovation Ministry and the ERDF within the frame of the project ‘Estimación de la energía generada por módulos fotovoltaicos de capa delgada: influencia del espectro’ under expedient code ENE2008-05098/ALT. This work was also supported by the Centre for Advanced Studies in Energy and Environment (University of Jaén) within the frame of the project ‘Caracterización y modelado de las irradiancias espectrales global sobre plano inclinado y directa normal mediante técnicas estadísticas y de inteligencia artificial’.

The authors are also grateful to Dr. Eduardo Fernández – Centre for Advanced Studies in Energy and Environment, University of Jaén, Spain for all his invaluable support while carrying out this work.

Finally, we thank the AERONET project, and more particularly Dr. Alados-Arboledas and Dr. Moreta for their effort in establishing and maintaining the Granada and Madrid sites, respectively.

References

- Alonso-Abella, M., Chenlo, F., Nofuentes, G., Torres-Ramírez, M., 2014. Analysis of spectral effects on the energy yield of different PV (photovoltaic) technologies: the case of four specific sites. *Energy* 67, 435–443.
- Baig, H., Fernández, E.F., Mallick, T.K., 2016. Influence of spectrum and latitude on the annual optical performance of a dielectric based BICPV system. *Sol. Energy* 124, 268–277.
- Betts, T.R., Infield, D.G., Gottschalg, R., 2004. Spectral irradiance correction for PV system yield calculations. In: Proc of 19th European Photovoltaic Solar Energy Conference, Paris, France.
- Cornaro, C., Andreotti, A., 2012. Influence of Average Photon Energy index on solar irradiance characteristics and outdoor performance of photovoltaic modules. *Prog. Photovoltaics Res. Appl.* 21 (5), 996–1003.
- Dimberger, D., Blackburn, G., Müller, B., Reise, C., 2015. On the impact of solar spectral irradiance on the yield of different PV technologies. *Sol. Energy Mater. Sol. Cells* 132, 431–442.
- Driesse, A., Dimberger, D., Reise, C., Reich, N.H., 2012. Spectrally selective sensors for PV system performance monitoring. In: Proc of the 38th IEEE Photovoltaic Specialists Conference, pp. 3294–3299.
- Fabero, F., Vela, N., Chenlo, F., 1995. Influence of solar spectral variations on the conversion efficiency of a-Si and m-Si PV devices: A yearly and hourly study. In: Proc of 13th European P Photovoltaic Solar Energy Conference, Nice, France, pp. 2281–2284.
- Faine, P., Kurtz, S., Riordan, C., Olson, J.M., 1991. The influence of spectral solar irradiance variations on the performance of selected single-junction and multijunction solar cells. *Sol. Cells* 31, 259–278.
- Fernández, F., Almonacid, P., Rodrigo, P., Pérez-Higueras, P., 2013. Model for the prediction of the maximum power of a high concentrator photovoltaic module. *Sol. Energy* 97, 12–18.
- Gonzalez, M.C., Carroll, J.J., 1994. Solar cells efficiency variations with varying atmospheric conditions. *Sol. Energy* 53, 395–402.
- Gracia Amillo, A.M., Huld, T., Vourlioti, P., Müller, R., Norton, M., 2015. Application of satellite-based spectrally-resolved solar radiation data to PV performance studies. *Energies* 8 (5), 3455–3488.
- Gueymard, C.A., 1995. Simple Model of the Atmospheric Radiative Transfer of Sunshine, version 2 (SMARTS2): Algorithms description and performance assessment. Rep. FSEC-PF-270-95, Florida Solar Energy Center.
- Gueymard, C.A., 2001. Parameterized transmittance model for direct beam and circumsolar spectral irradiance. *Sol. Energy* 71, 325–346.
- Gueymard, C.A., 2009. Daily spectral effects on concentrating PV solar cells as affected by realistic aerosol optical depth and other atmospheric conditions. In: Proc of SPIE, Optical Modeling and Measurements for Solar Energy Systems III, San Diego CA, vol. 7410, pp. 741007.
- Gueymard, C.A., 2014. Impact of on-site atmospheric water vapor estimation methods on the accuracy of local solar irradiance predictions. *Sol. Energy* 101, 74–82.
- Hegeudus, S., Luque, A., 2003. Handbook of Photovoltaic Science and Engineering. Wiley, Chichester.
- Hofmann, M., Vanicek, P., Haselhuhn, R., 2013. Is the average photon energy (APE) a suitable measure to describe the uniqueness of solar spectra? In: Proc of 29th European Photovoltaic Solar Energy Conference and Exhibition, Paris, France, pp. 3461–3466.
- Holben, B., Eck, T., Slutsker, I., Tanré, D., Buis, J., Setzer, A., Vermote, E., Reagan, J., Kaufman, Y., Nakajima, T., Lavenu, F., Jankowiak, I., Smirnov, A., 1998. AERONET-A federated instrument network and data archive for aerosol characterization. *Remote Sens. Environ.* 66 (1), 1–16.
- IEC 60904-7 (Ed. 3.0), 2008. Photovoltaic devices – Part 7: Computation of the spectral mismatch correction for measurements of photovoltaic devices. Geneva.
- IEC 60904-9 (Ed. 2.0), 2007. Photovoltaic devices – Part 9: Solar simulator performance requirements. Geneva.
- Ishii, T., Otani, K., Takashima, T., Xue, Y., 2013. Solar spectral influence on the performance of photovoltaic (PV) modules under fine weather and cloudy weather conditions. *Prog. Photovoltaics Res. Appl.* 21 (4), 481–489.
- Jardine, C., Betts, T., Gottschalg, R., Infield, D.G., Lane, K., 2002. Influence of spectral effects on the performance of multijunction amorphous silicon cells. In: Proc of PV in Europe – From PV Technology to Energy Solutions, Rome, Italy.
- Louwen, A., de Waal, A.C., van Sark, W.G.J.H.M., 2016. Evaluation of different indicators for representing solar spectral variation. In: Proc 43th IEEE Photovoltaic Specialists Conference, Portland, OR.
- Mavromatakis, F., Gueymard, C.A., Franghiadakis, Y., 2007. Improved total atmospheric water vapour amount determination from near-infrared filter measurements with sun photometers. *Atmos. Chem. Phys.* 7, 4613–4623.
- Minemoto, T., Takahashi, H., Nakada, Y., Takakura, H., 2010. Outdoor performance evaluation of photovoltaic modules using contour plots. *Curr. Appl. Phys.* 10, 257–260.
- Minemoto, T. et al., 2007. Effect of spectral irradiance distribution on the outdoor performance of amorphous Si/thin-film crystalline Si stacked photovoltaic modules. *Sol. Energy Mater. Sol. Cells* 91 (2–3), 120–122.
- Minemoto, T., Nakada, Y., Takahashi, H., Takakura, H., 2009. Uniqueness verification of solar spectrum index of average photon energy for evaluating outdoor performance of photovoltaic modules. *Sol. Energy* 83 (8), 1294–1299.
- Myers, D.R., 1989. Estimates of uncertainty for measured spectra in the SERI spectral solar radiation data base. *Sol. Energy* 43 (6), 347–353.
- Myers, D.R., Gueymard, C.A., 2004. Description and availability of the SMARTS spectral model for photovoltaic applications. In: Proc of Organic Photovoltaics V Conference, SPIE 5520, Denver, CO.
- Nann, S., Emery, K., 1992. Spectral effects on PV-device rating. *Sol. Energy Mater. Sol. Cells* 27 (3), 189–216.
- Nofuentes, G., García-Domingo, B., Muñoz, J.V., Chenlo, F., 2014. Analysis of the dependence of the spectral factor of some PV technologies on the solar spectrum distribution. *Appl. Energy* 113, 302–309.
- Nofuentes, G., De La Casa, J., Torres-Ramírez, M., Alonso-Abella, M., 2013. Solar spectral and module temperature influence on the outdoor performance of thin film PV modules deployed on a sunny inland site. *Int. J. Photoenergy* 2013, 620127.
- Nofuentes, G., Fuentes, M., Aguilera, J., Muñoz, J.V., 2009. An assessment on simple modeling approaches to the electric behavior of two CIS PV modules in a sunny climate. *J. Sol. Energy-T ASME* 131, 10.
- Norton, M., Gracia Amillo, A.M., Galleano, R., 2015. Comparison of solar spectral irradiance measurements using the average photon energy parameter. *Sol. Energy* 120, 337–344.
- Pearsall, N.M., Emery, K.A., Davies, M., 1986. Influence of reference cell and spectrum on the measurement of solar cells. In: Proc of 7th European Photovoltaic Solar Energy Conference, Seville, Spain, pp. 298–303.
- Riordan, C., Hulstrom, R., 1990. Outdoor spectral solar radiation variations and their relationship to photovoltaic device performance. *Curr. Top. Photovolt.* 4, 1–23.
- Schubert, F., Klameth, K., Darou, S., Spinner, D., 2015. Measurement uncertainties of a compact array spectrometer. *Energy Proc.* 77, 179–186.
- Sirisamphanwong, C., Ketjoy, N., 2012. Impact of spectral irradiance distribution on the outdoor performance of photovoltaic system under Thai climatic conditions. *Renew. Energy* 38, 69–74.
- Sutterlueti, J., Ransome, S., Kravets, R., Schreier, L., 2011. Characterising PV modules under outdoor conditions: what’s most important for energy yield? In: Proc of 26th European Photovoltaic Solar Energy Conference and Exhibition, Hamburg, Germany.
- Takahashi, H., Fukushige, S., Minemoto, T., Takakura, H., 2009. Output estimation of Si-based photovoltaic modules with outdoor environment and output map. *J. Cryst. Growth* 311 (3), 749–752.
- Torres-Ramírez, M., Elizondo, D., García-Domingo, B., Nofuentes, G., Talavera, D.L., 2015. Modelling the spectral irradiance distribution in sunny inland locations using an ANN-based methodology. *Energy* 86, 323–334.
- Torres-Ramírez, M., Nofuentes, G., Silva, J.P., Silvestre, S., Muñoz, J.V., 2014. Study on analytical modelling approaches to the performance of thin film PV modules in sunny inland climates. *Energy* 73, 731–740.
- Virtuani, D., Strepparava, G., Friesen, G., 2015. A simple approach to model the performance of photovoltaic solar modules in operation. *Sol. Energy* 120, 439–449.

- Wilk, H., 1997. Electricity yield of PV systems in different climates and dependence of module efficiency as a function of irradiance and other factors. In: Proc of 14th European Photovoltaic Solar Energy Conference, Barcelona, Spain.
- Wilson, H.R., 1986. Effect of solar spectral variation on solar cell short circuit current; Results of long-term continuous measurements. In: Proc of 7th European Photovoltaic Solar Energy Conference. Seville, Spain, pp. 309–313.
- Ye, J.Y., Reindl, T., Aberle, A.G., Walsh, T.M., 2014. Performance degradation of various PV module technologies in tropical Singapore. *IEEE J. Photovolt.* 4 (5), 1288–1294.
- Yoshida, S., Ueno, S., Kataoka, N., Takakura, H., Minemoto, T., 2013. Estimation of global tilted irradiance and output energy using meteorological data and performance. *Sol. Energy* 93, 90–99.